Structural, optical and electrical properties of Sn_xS_y thin films grown by spray ultrasonic

I. B. Kherchachi[†], A. Attaf, H. Saidi, A. Bouhdjer, H. Bendjedidi, Y. Benkhetta, and R. Azizi

Physics of Thin Films and Applications Laboratory (LPCMA), University of Biskra, BP 145 RP, Biskra 07000, Algeria

Abstract: Tin sulfide (Sn_xS_y) thin films were prepared by a spray ultrasonic technique on glass substrate at 300 ℃. The influence of deposition time $t = 2, 4, 6, 8$ and 10 min on different properties of thin films, such as (XRD), photoluminescence (PL) and (UV) spectroscopy visible spectrum and four-point were investigated. X-ray diffraction showed that thin films crystallized in SnS_2, SnS, and Sn_2S_3 phases, but the most prominent one is SnS_2. The results of the (UV) spectroscopy visible spectrum show that the film which was deposited at 4 min has a large transmittance of 60% in the visible region. The photoluminescence spectra exhibited the luminescent peaks in the visible region, which shows its potential application in photovoltaic devices. The electrical resistivity (ρ) values of Sn_xS_y films have changed from 8.1×10^{-4} to 1.62 Ω·cm with deposition time.

1. Introduction

Tin chalcogenides are attractive semiconductor materials and are potentially used as a solar cell[1], holographic recording medium[2], light-emitting diodes[3], electrical switching[4,5], lithium-ion battery due to its high theoretical capacities[6], gas-sensor[7,8] and optical material[7,9], etc. In the phase diagram of the Sn–S binary system, there are three known stoichiometric compounds, with different tin to sulfur ratios: SnS, Sn_2S_3 and SnS_2[10−12] that are the most interesting[13−15] materials according to a technological standpoint. In addition, the tin sulfide SnS has many advantages for photovoltaic applications such as the gap that can approach the optimum for the conversion of solar energy (1.50 eV)[16,17], low cost, non-natural toxic and is easily developed because these components are very abundant on earth[18]. Moreover, SnS_2 as an n-type semiconductor, has a layered hexagonal structure with a larger band gap varying (0.8–2.88 eV), it is a good light absorber (absorption coefficient of 10^4 cm^{-1})[5,19,20], it is known for its intriguing optical and electrical properties and potential applications[21]. Several deposition techniques have been used to prepare tin sulfide thin films, including: the chemical bath deposition method (CBD)[22], thermal evaporation[23], RF sputtering[24], electrochemical deposition[25,26], hot wall method[27], novel hydrothermal method[28], successive ionic layer adsorption and reaction method (SILAR)[29,30], pulse electro-deposition method[31], spray pyrolysis[32,33], electron beam evaporation[34], plasma-enhanced chemical vapor deposition (PECVD)[35], and dip coating method[36]. In this work, structural, optical and electrical properties of Sn_xS_y films were studied through using the spray ultrasonic method with different deposition times (2, 4, 6, 8 and 10 min).

2. Experimental procedure

Sn_xS_y thin films were deposited on glass substrates using the spray ultrasonic technique. The spraying solution consisted of a tin Chloride dehydrate ($SnCl_2 \cdot 2H_2O$) and a thiourea ($CS(NH_2)_2$). The molarity of sulfide (M_{Sn}) was 0.05 mol/L and the molarity of thiourea (M_S) was 0.1 mol/L; both of them were dissolved in methanol. The substrate temperature was 300 ℃, the solution flow rate was 50 mL/h, the distance between the nozzle and the substrate was 5 cm and all of them were kept constant. However, the spraying deposition time varied from 2 to 10 min.

The films were characterized by means of structural optical and electrical techniques. The X-ray diffraction studies were carried out using a D8 ADVANCED BRUKER diffractometer with a copper anode having a wavelength $\lambda = 1.5418$ Å. The UV–vis–NIR transmittance measurements were performed. An UV–vis–NIR (UVI-3101 PC SHIMADZU) spectrometer has been used in the range 300–900 nm for the calculations for the transmittance. The photoluminescence (PL) spectra of the samples were obtained from the excitation of the 325 nm. The electrical resistivity of films was measured by four-point.

3. Results and discussion

3.1. Structural studies

Figure 1 shows the variation of film thickness as a function of deposition time. At a low deposition time of 2 min, the nucleation step is very short, and with an increase in the deposition, the growth of the film becomes easier and linear. This indicates that the deposition of atoms on the first layer becomes faster with time; this was reported in the figure that inserts the variation of the deposition rate with deposition time.

Figure 2 shows the XRD patterns of Sn–S thin films grown at various deposition times, it can be seen that the films which are formed at 2 to 6 min show a peak corresponding to the SnS_2 hexagonal phase[37] (JCPDS card No 23-0677) with preferential orientation in the plane (001) around the angle $2\theta =$
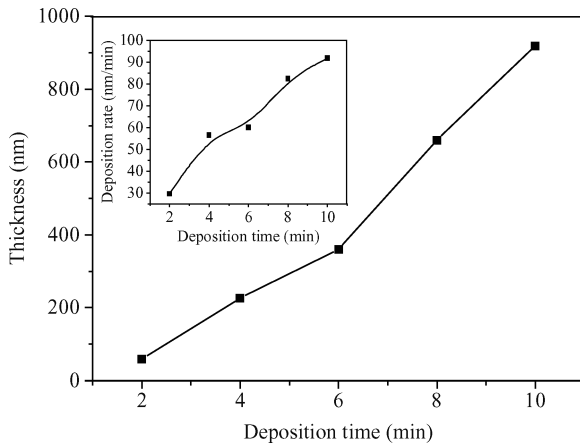
Figure 1. The variation of the films thickness and growth rate as a function of deposition time.

Figure 2. X-ray spectra of the samples of Sn_xS_y: SnS_2, Sn_2S_3, SnS.

15.02°. The films grown at 8 to 10 min and the previous one (2 to 6 min) show the same prominent peak corresponding to SnS_2 whereas other peaks observed at 8 min of 2θ values of 26.70°, 33.98° and 50.27° were found to match with reflections of minimum intensity from (111), (221) and (110) crystallographic planes of Sn_2S_3 and SnS_2 phase respectively. The peak seen at 10 min of 2θ values of 45.56° is found with reflections from the (002) plane of the SnS phase (JCPDS card No 390354). Similar results about the formation of the SnS_2 phase using the $SnCl_2 \cdot 2H_2O$ precursor has been observed by Reddy *et al.*[38, 39]; they found that the SnS_2 phase of Sn–S films obtained by spray pyrolysis became predominant as the temperature increases to 300 °C. Our results differ from those reported in the literature by Sajeesh *et al.*[33] for the films deposited by spraying solutions with Sn : S of 1 : 2; Sn_2S_3 is the main crystalline phase in the films grown at temperatures below 300 °C.

A prominent (001) peak indicates that the crystallite structure of Sn–S films is oriented with their *c*-axis perpendicular to the substrate plane, due to its surface energy and that the atoms will arrange themselves into the plane with the lowest surface energy[40]. However, it can be suggested that this low surface energy is referred by the increased deposition rate reported in Figure 1. From the experimental results and data taken from the JCPDS card No 23-0677, we see that there are slight differences between the positions of the peaks and the lattice parameters (*a* and *c*). This may be caused by the manifestation of a defect in the cell of the crystal, which causes local changes in the lattice parameters. The obtained results are reported in Table 1.

Information gleaned from the XRD profiles was used to evaluate the crystallite size (*D*) using Scherrer's formula[41−45]:

$$D = \frac{K\lambda}{\beta \cos \theta}, \tag{1}$$

where *k* is a constant (0.94), β is the full width half maximum (FWHM) value, λ is the wavelength of the CuKα radiation source ($\lambda = 1.5418$ Å), and θ is the Bragg angle. The strain (ε) developed in the film was estimated using the following relation[46]:
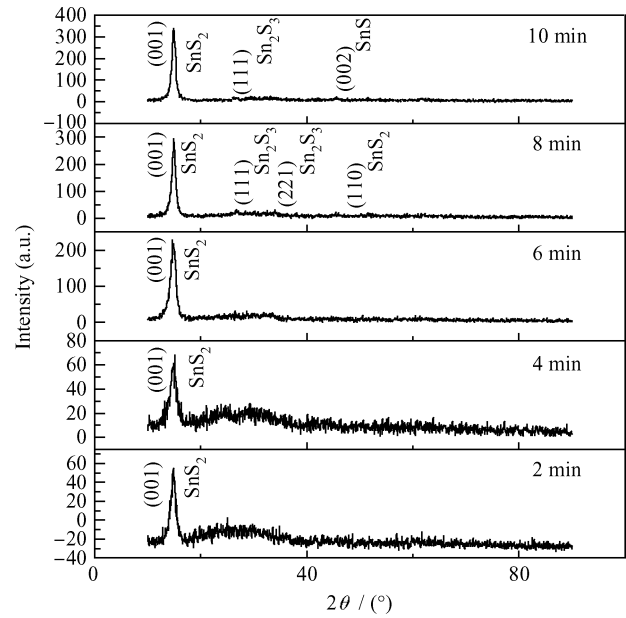
$$\varepsilon = \frac{\beta \cos \theta}{4}. \tag{2}$$

The variations of the crystallite size together with the film strain are reported in Figure 3. For the (001) plane, it was found that the crystallite size increased from 11.61 to 19.36 nm with increasing deposition time from 2 to 6 min and then it decreased to 11.22 nm for the deposition time of 10 min. These values are comparable to those reported by Panda *et al.*[36] and Wei *et al.*[47]. The reduction of the crystallite size which is between (8–10 min) is likely caused by the emergence of other phases SnS and Sn_2S_3 corresponding to (111), (110), (221) and (002) that lead to the detriment of orientation (001). In addition, this reduction can be attributed to the force decreasing between crystals attracting each other with the Van der Waals force because the substrate remained in the solution longer than necessary[48]. From these results we get to say that we have a weak restriction regime[46] because the crystallite size is very small, of the order of the rayon of an exciton in a bulk material (rayon of the exciton Bohr), less than 20 nm. By contrast, strain varies in the range $(1.87–3.24) \times 10^{-3}$ with the variation of the deposition time. The decrease in crystallite size in the thin layers of Sn_xS_y is responsible for the growth of the strain. The reduction of their sizes generates along the grain which shows stresses in the network[49].

Using crystallite size values, the dislocation density (δ), defined as the length of dislocation lines per unit volume of the crystal has been calculated by using the Williamson and Smallman's formula[50]:

$$\delta = \frac{1}{D^2}. \tag{3}$$

Moreover, the number of crystallites per unit surface area n_c has been calculated using the following formula[49]:

$$n_c = \frac{e}{D^3}, \tag{4}$$

where *e* is the film thickness, it is about 0.059–0.92 μm, and D is the crystallite size. The variations of the dislocation density and the number of crystallites are shown in Figure 4. As seen,
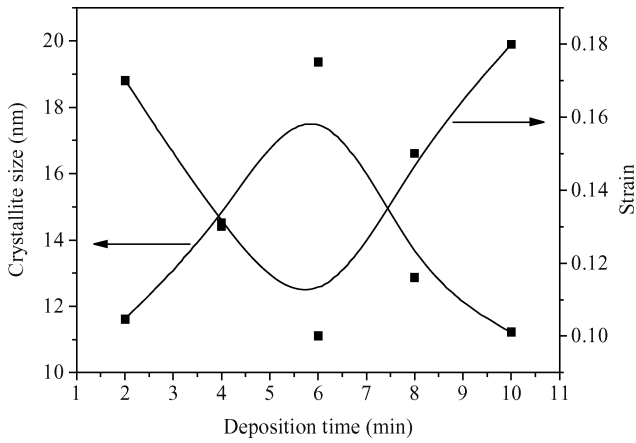
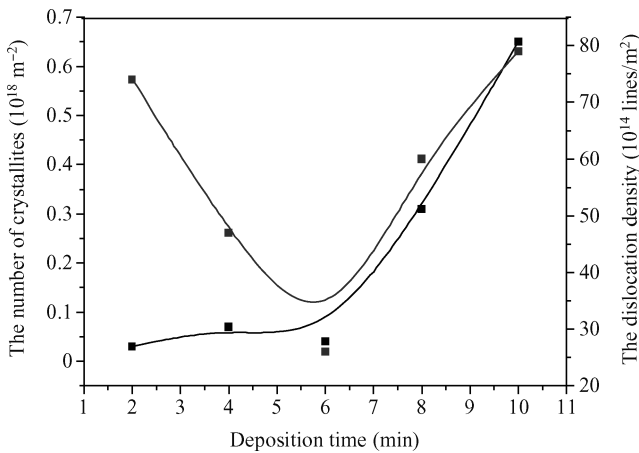Figure 3. Dependence of crystallite size and strain on deposition time.

Figure 4. The variation of dislocation density and the variation of the number of crystallites with the deposition time of Sn_xS_y thin films.

the number of crystallites increased with increasing deposition time. The same variation was observed by Guneri *et al.*[47]. The dislocation decreased with increasing deposition time (2–6 min) then increased with increasing deposition time. The preferential orientation of the dominant phase of the sample has been determined by means of the texture coefficient (TC) using the expression[51, 52]:

$$TC(hkl) = \frac{I(hkl)/I_0(hkl)}{\frac{1}{N}\sum_n I(hkl)/I_0(hkl)}, \qquad (5)$$

where $I_0(hkl)$ is the standard intensity of the (hkl) plane, $I(hkl)$ is the observed intensity of the (hkl) plane, N is the reflection number and n is the number of diffraction peaks. The results were presented in Table 1. From the texture coefficient calculations, it was found that the preferential orientation of deposited films with different deposition times, namely 2, 4, 6, 8, and 10 min, was the (001) orientation.

3.2. Optical studies

Figure 5 shows the optical transmittance measured in accordance with wavelength. The deposition time has a huge impact on optical transmittance of the films. Through the observation of Figure 5 we can see that there is a lack of interference
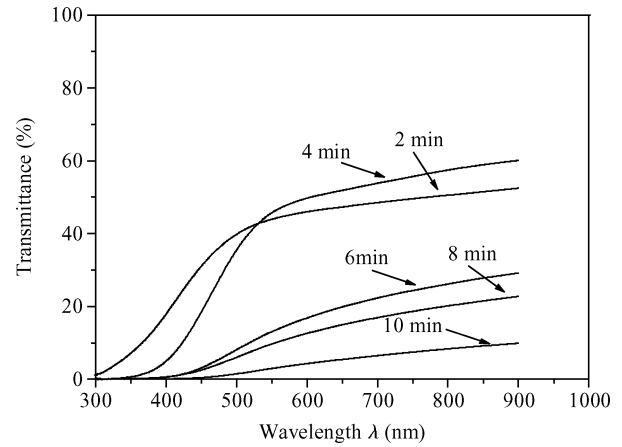

Figure 5. Transmission curves for Sn_xS_y at different deposition times.

fringes due to the multiple reflections[53]; the absence of these fringes in our films indicates that the texture appeared as rough. It can be observed that when the deposition time increases, the transmittance increases as well until 4 min, and decreases again with further deposition time increase; this reduction refers to the increase of thickness of films which is controlled by the deposition time. The transmittance in the visible region for the samples obtained from 2 to 10 min is around 10%–60%. The film deposited at 10 min has a higher absorbance than the others.

The plot of $(\alpha h\nu)^2$ versus $h\nu$ for Sn_xS_y thin film is shown in Figure 6. The linear nature of the graph indicates the existence of a direct transition. The gap energy is determined by extrapolating the straight portion of the plot to the energy axis. The gap energy (E_g) of our films was determined from the transmittance spectra using the Tauc relation[54]:

$$Ah\nu = (h\nu - E_g)^n, \qquad (6)$$

where A is a constant, E_g is the optical band gap of the material and the exponent $n = 1/2$ stands for the allowed direct transitions. On the other hand, we have used the Urbach energy (E_u), which is related to the disorder in the film network, as it is expressed as[55]:

$$A = A_0 \exp\frac{h\nu}{E_u}, \qquad (7)$$

where A_0 is a constant, $h\nu$ is the photon energy and E_u is the Urbach energy.

The variations of the calculated optical band gap and band tail width E_u with deposition time are reported together in the same graph (Figure 7). The optical band gap value is ranged from 2.73 to 2.85 eV, the value found is in the same order of the reported values in References [56, 57]. The optical band gap decreases with increasing deposition time. This decrease in optical band gap with an increase in deposition time can be attributed mainly by the increase in the film thickness. For SnS thin films that are deposited at near room temperature, the same results have been found in the previous research[58, 59]. While the Urbach energy varies inversely. The widening of the gap is because of the reduction of the urbach energy in the film[60].

The photoluminescence (PL) is one of the significant studies which can give us more important information on the crys-

Table 1. Structural parameters of spray ultrasonic Sn_xS_y films.

Depositiontime(min)	2θ (°)	Lattice parameters (Å)	hkl planes	TC	Lattice parameters (Å)	2θ (°)
		Sn_xS_y			JCPDS card reference No 23-0677	
2	14.95	$a = 5.932$	(001)	1	$a = 5.899$	15.02
		$c = 3.638$				
4	14.85	$a = 5.760$	(001)	1	$c = 3.648$	26.58
		$c = 3.533$				
6	15.04	$a = 5.927$	(001)	1		33.79
		$c = 3.636$				
8	14.97	$a = 5.917$	(001)	1.04		49.96
	26.70	$c = 3.630$	(111)	0.72		
	33.98		(221)	2.04		
	50.27		(110)	0.18		
10	14.93	$a = 5.931$	(001)	2.01		45.49
	26.73	$c = 3.638$	(111)	0.73		
	45.56		(002)	0.24		
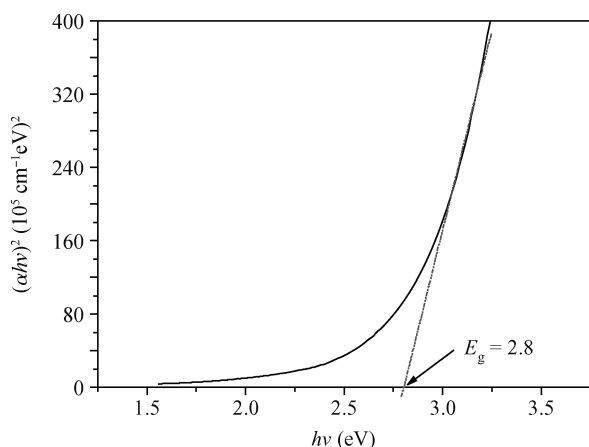
Figure 6. The plot of $(\alpha h\upsilon)^2$ versus $(h\upsilon)$ for Sn_xS_y film.
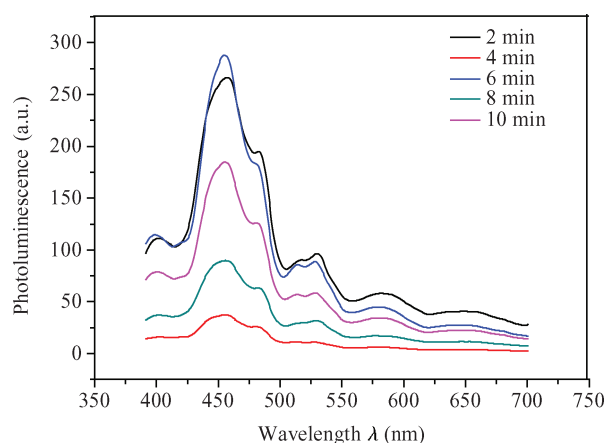

Figure 8. (Color online) PL spectra versus wavelength λ plot of Sn_xS_y thin films prepared at different deposition times.
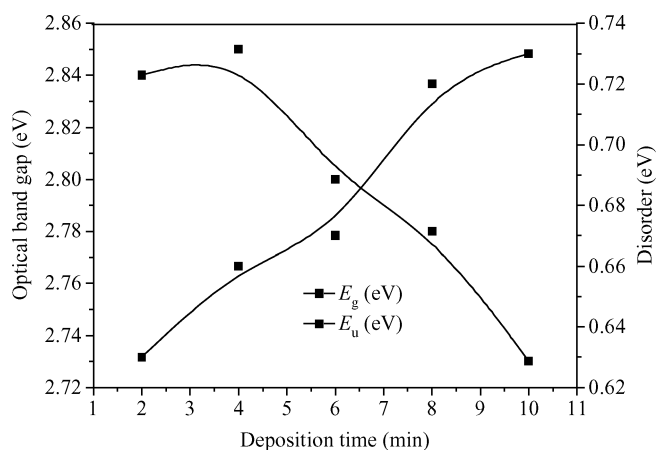

Figure 7. The variation of optical band gap and disorder of Sn_xS_y at different deposition time.

peak at 590 nm for tin disulfide thin films. While, Deshpande *et al.*[56] have observed two emission peaks of PL attributed to 549.78 nm (green) and 700.28 nm (red) emission of SnS_2. In our study, the strong PL peak centered at 455 nm is the maximum for a sample prepared with a deposition time of 6 min; this peak corresponds to the radiative recombination of bound excitons, whereas the explanation for the origin of the broad peaks at 530, 583 and 648 nm (the most intense form of samples prepared at the deposition time of 2 min) may be from the inner deep level emission[62]. This deep level arises because of the stoichiometric variation in the SnS_2 phase. Another possible explanation can be ascribed to the emission from sulfide vacancies V_S or interstitial tin atoms I_T, which are considered to be the localizer states in the optical band gap. Another researcher has referred the origin of broad peaks to the impurities and native defects, such as interstitial tin atoms[56].

3.3. Electrical studies

The electrical resistivity (ρ) of the films formed at different deposition times is shown in Figure 9. According to this figure, resistivity decreased slightly from 8.1×10^{-4} to 2×10^{-4} Ω·cm with increasing deposition time from 2 to 6 min and after that deposition time, it increased suddenly to the value of 1.62

tal quality and purity of the material. The room temperature PL emission spectra of the Sn_xS_y thin films, deposited with different deposition time $t = 2, 4, 6, 8$ and 10 min are demonstrated in Figure 8. PL spectra consist of four emission peaks centered at about 455(blue), 530 (green), 583 (yellow) and 648 (red), with energy corresponding to all the observed emission peaks 2.73, 2.34, 2.12 and 1.91 eV. Yang *et al.*[61] have reported a PL
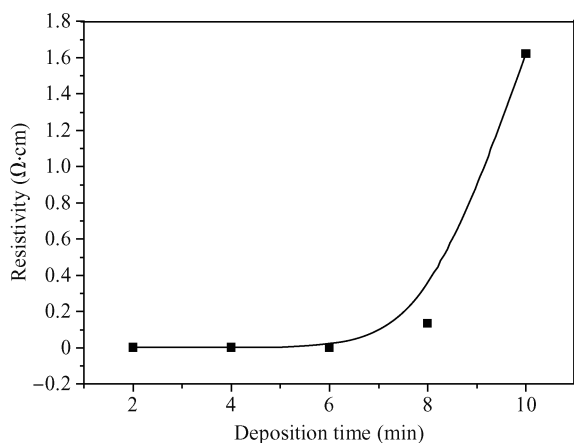
Figure 9. The variation of electrical resistivity with different deposition time.

Ω·cm. The lowest resistivity (2×10^{-4} Ω·cm) obtained for the deposition time equals 6 min, which is due to the better crystallinity of the films prepared at this deposition time. These results are strongly supported by XRD analysis (Figure 2), which indicates that the films grown at 6 min have a larger grain size than the other films. An increase in grain size of this film leads to reduced grain boundary scattering, and thus a decrease in electrical resistivity. However, the higher electrical resistivity of the films formed at a deposition time longer than 6 min refers to the smaller grain size. Similar interpretations were obtained in SnS thin films deposited by the chemical bath deposition technique with increasing deposition time by Guneri *et al.*[47]. Although, the crystallite size of the films deposited at 8 and 10 min is close to that deposited at 2 and 4 min, the resistivity of the films deposited at 8 and 10 min is higher than those deposited at 2 and 4 min. This result is probably due to the presence of SnS_2 and other new phases like SnS and Sn_2S_3. This later might be responsible for the higher resistivity. Sajeesh[34] reported the similar regard. In their study, they explained that the high value of resistivity of the films prepared below 300 ℃ is a result of the presence of the mixed valent compound Sn_2S_3 presence. Also Reddy *et al.*[38] interpreted the high resistivity of the film deposited for temperature < 300 ℃ due to the appearance of SnS_2 and Sn_2S_3.

4. Conclusion

In this study we investigated the influence of deposition time on the structural, optical and electrical properties of tin sulfide prepared by ultrasonic spray on glass substrates at a temperature of 300 ℃. Firstly, from the X-ray diffraction, we found that our layers have a preferred orientation (001) of the SnS_2 phase and other small peaks corresponding to the SnS and Sn_2S_3 phases occurred only in 8 and 10 min; these results indicate a good crystalline structure with the (001) orientation. Secondly, we found that the variation of the deposition time affected the optical properties of the films of Sn_xS_y and the higher absorbance was detected for the deposition time of 10 min; this leads us to note that 10 min is an optimal value. The photoluminescence spectra exhibited the luminescent peaks in the visible region, which shows its potential ap-

plication in photovoltaic devices. Thirdly, the electrical resistivity (ρ) increased when the SnS and Sn_2S_3 phases appeared. Finally, the ideal condition for better solar cell efficiency is increasing the deposition time.

References

[1] Li H, Zhang Q, Pan A, et al. Single-crystalline $Cu_4Bi_4S_9$ nanoribbons: facile synthesis, growth mechanism, and surface photovoltaic properties. Chem Mater, 2011, 23: 1299

[2] Niasari M S, Ghanbari D, Davar F. Shape selective hydrothermal synthesis of tin sulfide nanoflowers based on nanosheets in the presence of thioglycolic acid. Alloys and Compounds, 2010, 492: 570

[3] Wang Z, Liu J, Dai Y, et al. Dimethyl sulfide photocatalytic degradation in a light-emitting-diode continuous reactor: kinetic and mechanistic study. Chen Ind Eng Chem Res, 2011, 50: 7977

[4] Agarwal A, Patel P D, Lakshminarayana D. Single crystal growth of layered tin monoselenide semiconductor using a direct vapour transport technique. J Cryst Growth, 1994, 142: 344

[5] Domingo G, Itoga R S, Cannewurf C R. Fundamental optical absorption in SnS_2 and $SnSe_2$. Phys Rev, 1966, 143: 536

[6] Momma T, Shiraishi N, Yoshizawa A, et al. SnS_2 anode for rechargeable lithium battery. Power Sources, 2001, 97: 198

[7] Hu Xianghua, Song Guosheng, Li Wenyao, et al. Phase-controlled synthesis and photocatalytic properties of SnS, SnS_2 and SnS/SnS_2 heterostructure nanocrystals. Materials Research Bulletin, 2013, 48: 2325

[8] Shi W D, Huo L H, Wang H S, et al. Hydrothermal growth and gas sensing property of flower-shaped SnS_2 nanostructures. Nanotechnology, 2006, 17: 2918

[9] Bertrand Y, Barski A, Pinchaux R. Experimental valence-band structure of tin disulfide SnS_2. Phys Rev B, 1985, 31: 5494

[10] Burton L, Colombara D, Abellon R, et al. Synthesis, characterization, and electronic structure of single-crystal SnS, Sn_2S_3, and SnS_2. Chem Mater, 2013, 25: 4908

[11] Price L S, Parkin I P, Hardy A, et al. Atmospheric pressure chemical vapor deposition of tin sulfides (SnS, Sn_2S_3, and SnS_2) on glass. Chem Mater, 1999, 11: 1792

[12] Burton L A, Walsh A. Phase stability of the earth-abundant tin sulfides SnS, SnS_2, and Sn_2S_3. Phys Chem, 2012, 116: 24262

[13] Chattopadhyay T, Werner A, von Schnering H G. Temperature and pressure induced phase transition in IV–VI compounds. Rev Phys Appl, 1984, 19: 807

[14] Wiedemeier H, Von Schnering H G. Refinement of structure of GeS, GeSe, SnS and SnSe. Z Krist, 1978, 148: 295

[15] Wyckoff R. Crystal structure. London: Interscience Pub, 1963

[16] Gao C, Shen H, Sun L. Preparation and properties of zinc blende and orthorhombic SnS films by chemical bath deposition. Appl Surf Sci, 2011, 257: 6750

[17] Yang J, Tian Q, Chen Z, et al. Synthesis and characterization of tin disulfide hexagonal nanoflakes via solvothermal decomposition. Mater Lett, 2012, 67: 32

[18] Yang C, Wang W, Shan Z, et al. Preparation and photocatalytic activity of high-efficiency visible-light-responsive photocatalyst SnS_x/TiO_2. Solid State Chem, 2009, 182: 807

[19] Acharya S, Srivastava O N. Electronic behaviour of SnS_2 crystals. Phys Status Solidi, 1981, 65: 717

[20] Thangaraju B, Kaliannan P. Spray pyrolytic deposition and characterization of SnS and SnS_2 thin films. Phys D Appl Phys, 2000, 33: 1054

[21] Zhang Y C, Du Z N, Li S Y, et al. Novel synthesis and high visible light photocatalytic activity of SnS_2 nanoflakes from

SnCl$_2$·2H$_2$O and S powders. Appl Catal B, 2010, 95: 153

[22] Ragina A J, Preetha K C, Murali K V, et al. Wet chemical synthesis and characterization of tin sulphide thin films from different host solutions. Adv Appl Sci Res, 2011, 2: 438

[23] Priyal J, Arun P. Parameters influencing the optical properties of SnS thin films. Journal of Semiconductors, 2013, 34(9): 093004

[24] Hartman K, Johnson J L, Bertoni M I, et al. SnS thin-films by RF sputtering at room temperature. Thin Solid Films, 2011, 519: 7421

[25] Mariappan R, Mahalingam T, Ponnuswamy V. Preparation and characterization of electrodeposited SnS thin films. Optik, 2011, 122: 2216

[26] Kamel M M, Ibrahim M M. Electrochemical deposition and characterization of SnS thin films. Solid State Electrochem, 2011, 15: 683

[27] Bashkirov S A, Gremenok V F, Ivanov V A. Physical properties of SnS thin films fabricated by hot wall deposition. Fizika i Tekhnika Poluprovodnikov, 2011, 45(6): 765

[28] Zhu H, Yang D, Ji Y, et al. Two-dimensional SnS nanosheets fabricated by a novel hydrothermal method. Mater Sci, 2005, 40: 591

[29] Ghosh B, Das M, Banerjee P, et al. Fabrication and optical properties of SnS thin films by SILAR method. Appl Surf Sci, 2008, 254: 6436

[30] Sankapal B R, Mane R S, Lokhande C D. Successive ionic layer adsorption and reaction (SILAR) method for the deposition of large area (10 cm^2) tin disulfide (SnS$_2$) thin films. Res Bull, 2000, 35: 2027

[31] Cheng S, Chen Y, He Y, et al. The structure and properties of SnS thin films prepared by pulse electro-deposition. Mater Lett, 2007, 61: 1408

[32] Reddy N K, Reddy K T R. Growth of polycrystalline SnS films by spray pyrolysis. Thin Solid Films, 1998, 325: 4

[33] Sajeesh T H, Warrier A R, Kartha C S, et al. Optimization of parameters of chemical spray pyrolysis technique to get n and p-type layers of SnS. Thin Solid Films, 2010, 518: 4370

[34] Tanussevski A, Poelman D. Optical and photoconductive properties of SnS thin films prepared by electron beam evaporation. Solar Energy Materials and Solar Cells, 2003, 80: 297

[35] Akkari A, Reghima M, Guasch C, et al. Effect of deposition time on physical properties of nanocrystallized SnS zinc blend thin films grown by chemical bath deposition. Adv Mater Res, 2011, 324: 101

[36] Panda S K, Antonakos A, Liarokapis E, et al. Optical properties of nanocrystalline SnS$_2$ thin films. Mat Res Bull, 2007, 42: 576

[37] Khelia C, Boubaker K, Nasrallah T B, et al. Morphological and thermal properties of β-SnS$_2$ sprayed thin films using Boubaker polynomials expansion. Alloys and Compounds, 2009, 477: 461

[38] Reddy K T R, Reddy P P, Miles R W, et al. Investigations on SnS films deposited by spray pyrolysis. Opt Mater, 2001, 17: 295

[39] Reddy N K, Reddy K T R. SnS films for photovoltaic applications: physical investigations on sprayed Sn$_x$S$_y$ films. Physica B, 2005, 368: 25

[40] Cheng L L, Liu M H, Wang M X, et al. Preparation of SnS films using solid sources deposited by the PECVD method with controllable film characters. Alloys and Compounds, 2012, 545: 122

[41] Maissel L I, Glang R. Handbook of thin film technology. New York: McGraw Hill, 1970

[42] Warren B E. X-ray diffraction. New York: Dover, 1990

[43] Reddy K T R, Reddy N K, Miles R W. Photovoltaic properties of SnS based solar cells. Solar Energy Materials & Solar Cells, 2006, 90: 3041

[44] Devika M, Reddy K T R, Reddy N K, et al. Microstructure dependent physical properties of evaporated tin sulfide films. Appl Phys, 2006, 100: 023518

[45] Qiao Z, Latz R, Mergl D. Thickness dependence of In$_2$O$_3$:Sn film growth. Thin Solid Films, 2004, 466: 250

[46] Chopra K L. Thin film phenomena. New York: McGraw-Hill, 1969

[47] Wei R, Zhou T, Hu J, et al. Glutatione modified ultrathin SnS$_2$ nanosheets with highly photocatalytic activity for waste water treatment. Materials Research Express, 2014, 1: 025018

[48] Guneri E, Ulutas C, Kirmizigul F, et al. Effect of deposition time on structural, electrical and optical properties of SnS thin films deposited by chemical bath deposition. Appl Surf Sci, 2010, 257: 1189

[49] Jeyaprakash B G, Kumar R A, Kesavan K, et al. structural and optical characterization of spray deposited SnS thin film. American Science, 2010, 6: 3

[50] Williamson G B, Smallman R C. Dislocation densities in some annealed and cold-worked metals from measurements on the X-ray debye-scherrer spectrum. Philos Mag, 1956, 1(1): 34

[51] Gurumurugan K, Mangalaraj D, Narayandass S K, et al. Characterisation of transparent conducting CDO films deposited by spray pyrolysis. Semicond Sci Technol, 1994, 9: 1827

[52] Eze F C. Oxygen partial pressure dependence of the structural properties of CdO thin films deposited by a modified reactive vacuum evaporation process. Mater Chem Phys, 2005, 89: 205

[53] Ray C, Karanjai K, DasGupta D. Structure and photoconductive properties of dip-deposited SnS and SnS$_2$ thin films and their conversion to tin dioxide by annealing in air. Thin Solid Films, 1999, 350: 72

[54] Pankove J I. Optical processes in semiconductors. New York: Dover, 1975

[55] Benramache S, Benhaoua B, Belahssen O. The crystalline structure, conductivity and optical properties of Co-doped ZnO thin films. Optik, 2014, 125: 5864

[56] Deshpande N G, Sagade A A, Gudage Y G, et al. Growth and characterization of tin disulfide (SnS$_2$) thin film deposited by successive ionic layer adsorption and reaction (SILAR) technique. Alloys Compd, 2007, 436: 421

[57] Parasyuk O V, Olekseyuk I D, Piskach L V, et al. Phase relations in the Ag$_2$S–CdS–SnS$_2$ system and the crystal structure of the compounds. Alloys Compd, 2005, 399: 173

[58] Ogah O E, Zoppi G, Forbes I, et al. Thin films of tin sulphide for use in thin film solar cell devices. Thin Solid Films, 2009, 517: 4702

[59] Selim M S, Gouda M E, El-Shaarawy M G, et al. Effect of thickness on optical properties of thermally evaporated SnS films. Appl Sci Res, 2011, 7(6): 955

[60] Rao T P, Kumar C S. Effect of thickness on structural, optical and electrical properties of nanostructured ZnO thin films by spray pyrolysis. Appl Surf Sci, 2009, 255: 4579

[61] Yang Q, Tang K, Wang C, et al. A hexane solution deposition of SnS$_2$ films from tetrabutyltin via a solvothermal route at moderate temperature. Thin Solid Films, 2003, 436: 203

[62] Kiruthigaa G, Manoharan R C, Dhanapandian S. Role of temperature on the growth of SnS$_2$ nanoflakes synthesized by solid state reaction. International Recent Scientific Research, 2014, 5(4): 796